Geophys. J. Int. (2005) **163,** 1–9 doi: 10.1111/j.1365-246X.2005.02714.x

Sensitivity of electrical resistivity tomography data to electrode position errors

Greg A. Oldenborger, Partha S. Routh and Michael D. Knoll

Department of Geosciences, Boise State University, 1910 *University Drive, Boise, ID* 83725*, USA. E-mail: greg@cgiss.boisestate.edu*

Accepted 2005 June 17. Received 2005 May 5; in original form 2005 January 25

SUMMARY

Limitations of imaging using electrical resistivity tomography (ERT) arise because of the difficulty of quantifying the reliability of tomographic images. A major source of uncertainty in tomographic inversion is data error. Data error due to electrode mislocations is characterized by the sensitivity of electrical potential to both source and receiver positions. This sensitivity is described by a scattering-type equation and, therefore, depends not only on source–receiver separation, but also on the location and magnitude of contrasts in electrical conductivity. At the overlapping scales of near-surface environmental and engineering geophysical surveys, for which electrodes may be close to the target and experiment dimensions may be on the same order as those of the target, errors associated with electrode mislocations can significantly contaminate the ERT data and the reconstructed electrical conductivity. For synthetic experiments, variations in the data due to electrode mislocation are comparable in magnitude to typical experimental noise levels and, in some cases, may overwhelm variations in the data due to changes in material properties. Furthermore, the statistical distribution of electrode mislocation errors can be complicated and multimodal such that bias may be introduced into the ERT data. The resulting perturbations of the reconstructed electrical conductivity field due to electrode mislocations can be significant in magnitude with complex spatial distributions that are dependent both on the model and the experiment.

Key words: borehole geophysics, electrical resistivity, hydrology, potential field, sensitivity, tomography.

INTRODUCTION

The 3-D direct-current (DC) electrical resistivity tomography (ERT) experiment involves the reconstruction of electrically heterogeneous earth models from measurements of the electrical potential arising from application of a current source. The ERT method has proven to be a valuable geophysical tool for imaging hydrothermal alteration (Shima 1992), epithermal mineral prospects (Ellis & Oldenburg 1994), moisture content (Yeh *et al.* 2002), fracture flow paths (Slater *et al.* 1996), hydraulic barriers (Daily & Ramirez 2000) and dynamic processes such as vadose zone water movement (Binley *et al.* 2002), steam injection (Ramirez *et al.* 1993), air sparging (LaBrecque *et al.* 1999) and contaminant transport (Newmark *et al.* 1998).

Despite the successes of ERT, work is required to address limitations of inverted electrical conductivity distributions for providing reliable and especially stand-alone information about subsurface properties. A major source of uncertainty in tomographic inversion is data error, which can be manifest as inaccurate inverse results or artefacts (Gough & Sekii 2002). Poor understanding of the origins of data error results in a poor understanding of inversion artefacts and the consequence is a lack of confidence in tomographic images for practical interpretation.

One potential source of ERT data error is mislocation of electrodes due, for example, to inaccuracies of electrode string construction, placement errors, surveying errors, or deviation of boreholes and direct-push technologies. For conventional large-scale applications of the DC resistivity technique, the common perception is that exact electrode position information is not critical to an accurate and successful experiment or consequent data interpretation. However, in the context of robust inversion development, Morelli & LaBrecque (1996) illustrate that errors in electrode position significantly affect the ability to construct a reliable electrical conductivity field. Zhou & Dahlin (2003) present a more comprehensive investigation of electrode position errors for 2-D surface resistivity experiments. They develop expressions for the perturbation of the homogeneous geometric factor for several 2-D survey geometries in response to electrode spacing errors. For heterogeneous models, they perform synthetic inversions to demonstrate that spacing errors result in near-electrode variations of the reconstructed electrical conductivity field, the magnitudes of which are strongly dependent on the array type but may exceed 20 per cent.

To our knowledge, these are the only investigations of the effects of electrode position error on electrical resistivity data or inversions. In a similar study of airborne electromagnetic data error, Walker (1999) investigated the effect of flight height on inverted

conductivity images. Further, determination of exact source location is the central problem of earthquake hypocentre location (Aki & Lee 1976), and it is well known in the realms of seismic and radar traveltime tomography that small errors associated with the mislocation of sources and receivers may overwhelm variations in the data due to changes in velocity (Maurer 1996; Vasco *et al.* 1997).

Given the possibility of ERT data error resulting from electrode mislocation, assessment of the accuracy of heterogeneous conductivity fields recovered from these data requires characterizing the dependence of the data on electrode position. We quantify this dependence via the sensitivity of electrical potential to source and receiver position. Our position sensitivity calculations allow for prediction of the systematic error associated with electrode mislocations. These error predictions can be used to compare survey designs or as part of the *a priori* information that dictates data weighting and, thus, data fitting in an inverse paradigm. For a synthetic example, we demonstrate how the local linearized Fréchet derivative of the forward operator can be used to map electrode mislocation error (or any systematic data error) to artefacts in the estimated electrical conductivity.

THEORETICAL DEVELOPMENT

For the ERT experiment, the data $d(\mathbf{r})$ are a non-linear function of the model m according to $d(\mathbf{r}) = f(m)$. The observed data are inevitably contaminated by error, which we assume to be comprised of a random uncorrelated component e and a systematic component e^{s} such that $d^{\mathrm{obs}} = f(m) + e^{\mathrm{s}} + e$ (LaBrecque & Yang 2001). In an inverse context, unbiased errors in the data blur the region of model space that is compatible with the data, whereas bias introduced by e^{s} may shift the regions of resolvable model space. Consider minimization of the least-squares data objective function $\psi_d = \|f(m) + e^{\mathrm{s}} - d^{\mathrm{obs}}\|^2$. In the event that an estimate of e^{s} can be predicted, it can be incorporated into a data weighting operator W such that the objective function becomes $\psi'_d = \|W[f(m) - d^{\mathrm{obs}}]\|^2$. Gough & Sekii (2002) demonstrate that incorporation of e^{s} during inversion in terms of data weighting can mitigate inaccuracies in the recovered model. In the event that systematic errors are unaccounted for, they will map to artefacts Δm in the recovered model according to minimization of $\psi_d = \|f(m + \Delta m) - d^{\mathrm{obs}}\|^2$ such that $e^{\mathrm{s}} \approx J\Delta m$ where $J = \partial f/\partial m$ is the local linearized Fréchet derivative of the forward operator f.

For the ERT experiment, electrode mislocations will contribute to systematic error in a manner that can be predicted by the sensitivity of the electrical potential to source and receiver position. The general ERT differential equation and boundary condition are given by

$$-\nabla \cdot [\sigma(\mathbf{r})\nabla\phi(\mathbf{r})] = I\delta(\mathbf{r} - \mathbf{r}_{\mathrm{s}}) \qquad \text{within } V, \tag{1a}$$

$$\alpha(\mathbf{r})\phi + \beta(\mathbf{r})\partial\phi/\partial n = 0 \qquad \text{on } S, \tag{1b}$$

where ϕ is the electrical potential (hereafter potential), σ is the electrical conductivity (hereafter conductivity), $I\delta(\mathbf{r} - \mathbf{r}_{\mathrm{s}})$ is the pole–source function with current strength I, $\mathbf{r} = x\hat{\mathbf{i}} + y\hat{\mathbf{j}} + z\hat{\mathbf{k}}$ is the receiver position vector, $\mathbf{r}_{\mathrm{s}} = x_{\mathrm{s}}\hat{\mathbf{i}} + y_{\mathrm{s}}\hat{\mathbf{j}} + z_{\mathrm{s}}\hat{\mathbf{k}}$ is the source position vector and $\mathbf{n}$ is the outward normal vector to the surface boundary S of domain V. Since the differential operator is linear in ϕ, the response to any source array can be built from a summation of solutions for a series of pole sources (i.e. the principle of superposition).

By analogy to the problem of determining the sensitivity of ERT data with respect to electrical conductivity, we can attempt to determine the position sensitivity via any of three general approaches (e.g. McGillivray & Oldenburg 1990; Spitzer 1998): finite-difference perturbation, the sensitivity equation, or an adjoint Green's function solution. However, the development of sensitivity to position is unique in that position is an implicit component of both the differential operator and the source function of the DC electrical eq. (1).

The most straightforward of the three approaches, finite-differencing, involves repeated forward solutions for perturbed source and receiver locations. However, we would prefer a formulation of the sensitivity of potential to changes in source and receiver position that does not depend on choice of an arbitrary mislocation value and delivers some insight into the nature of the sensitivity. To this effect, we briefly discuss the results of the sensitivity and adjoint solutions. The significant results are that sensitivity to position obeys a scattering-type equation and both the sensitivity equation and adjoint solution for position sensitivity ultimately reduce to a finite-difference solution for practical ERT applications.

For a particular source position, the horizontal component of the source sensitivity equation is given by

$$-\nabla \cdot \left[\sigma(\mathbf{r})\nabla\frac{\partial\phi}{\partial x_{\mathrm{s}}}\right] = I\frac{\partial}{\partial x_{\mathrm{s}}}\delta(\mathbf{r} - \mathbf{r}_{\mathrm{s}}) \qquad \text{within } V, \tag{2a}$$

$$\alpha(\mathbf{r})\partial\phi/\partial x_{\mathrm{s}} + \beta(\mathbf{r})\frac{\partial}{\partial n}\partial\phi/\partial x_{\mathrm{s}} = 0 \qquad \text{on } S, \tag{2b}$$

where conductivity is not a function of source position. To evaluate the derivative on the delta function, we expand eq. (2) to Poisson's equation

$$-\nabla^2\frac{\partial\phi}{\partial x_{\mathrm{s}}} = \frac{I}{\sigma(\mathbf{r})}\frac{\partial}{\partial x_{\mathrm{s}}}\delta(\mathbf{r} - \mathbf{r}_{\mathrm{s}}) + \frac{\nabla\sigma}{\sigma(\mathbf{r})} \cdot \nabla\frac{\partial\phi}{\partial x_{\mathrm{s}}}, \tag{3}$$

and apply the wholespace Green's function for the Laplacian to obtain the integral solution for the sensitivity of wholespace potential ϕ_0 to the source position:

$$\frac{\partial\phi_0}{\partial x_{\mathrm{s}}} = \frac{I}{4\pi\sigma_{\mathrm{s}}}\frac{x - x_{\mathrm{s}}}{|\mathbf{r} - \mathbf{r}_{\mathrm{s}}|^3} + \frac{1}{4\pi}\int_{V'}\frac{\nabla\sigma(\mathbf{r}') \cdot \nabla(\partial\phi_0/\partial x_{\mathrm{s}})}{|\mathbf{r} - \mathbf{r}'|}\,\mathrm{d}V'. \tag{4}$$

This equation is a scattering-type equation with a homogeneous primary term and a secondary integral scattering term. Not only does the sensitivity depend on the source-receiver separation, but it also depends on the location and magnitude of contrasts in electrical conductivity due to the phenomenon of charge accumulation (Li & Oldenburg 1991).

Scattering equations can be difficult to solve and a Born approximation is expected to be inadequate in the presence of realistic conductivity contrasts (Hohmann & Raiche 1988, p. 471). Alternatively, we can pursue an approach to determining the sensitivity that uses the Green's function to solve for the perturbation in potential associated with a perturbation in the parameter of interest (McGillivray & Oldenburg 1990). The self-adjoint Green's function is defined as the solution to the differential equation in response to an impulse source:

$$-\nabla \cdot [\sigma(\mathbf{r})\nabla G(\mathbf{r}, \mathbf{r}')] = \delta(\mathbf{r} - \mathbf{r}'). \tag{5}$$

Due to the point nature of the electrical source in eq. (1), the potential solution is given by a scaled Green's function $\phi(\mathbf{r}, \mathbf{r}') = IG(\mathbf{r}, \mathbf{r}')$. Perturbing the DC electrical equation with respect to horizontal source position yields

$$-\nabla \cdot [\sigma(\mathbf{r})\nabla\delta\phi] = I\delta(\mathbf{r} - \mathbf{r}_{\mathrm{s}} - \delta\mathbf{r}_{\mathrm{s}}) - I\delta(\mathbf{r} - \mathbf{r}_{\mathrm{s}}), \tag{6}$$

for which the perturbation in position cannot be isolated. Applying the Green's function to the perturbation equation results in $\partial\phi(\mathbf{r}, \mathbf{r}_{\mathrm{s}})/\partial x_{\mathrm{s}} = I\partial G(\mathbf{r}, \mathbf{r}_{\mathrm{s}})/\partial x_{\mathrm{s}}$ in the limit of the perturbation going

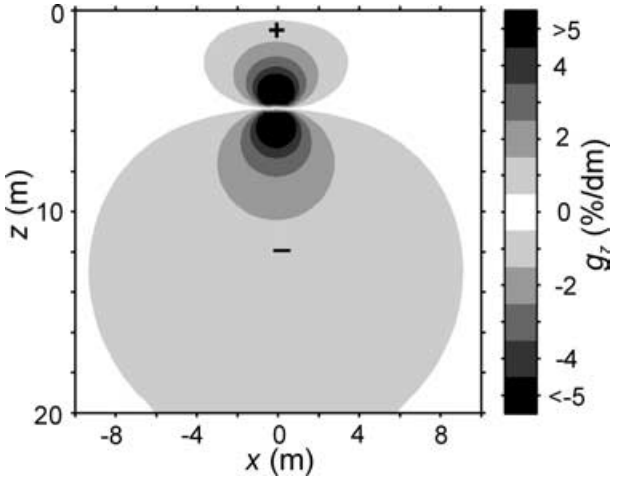

Figure 1. Normalized sensitivity of potential to receiver electrode position in the vertical direction for a pole–pole experiment. The current source is located at $x = 0$ m, $z = 5$ m within a 3-D half-space. For example, a 10 cm vertical mislocation of a common-hole receiver pole at 10 m depth would result in approximately 2 per cent error in the datum.

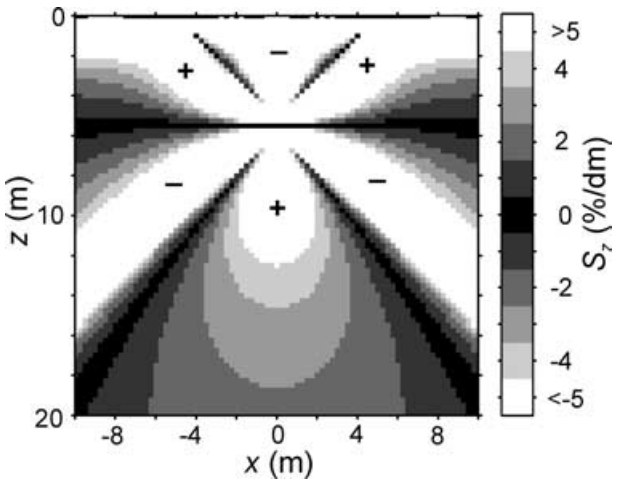

Figure 2. Normalized sensitivity of potential difference to vertical position of the receiver dipole for a vertical 1 m dipole–dipole experiment. The current dipole is centred at $x = 0$ m, $z = 5.5$ m. Sensitivities are plotted at the receiver dipole centre. For example, a 10 cm vertical mislocation of a common-hole receiver dipole at 10 m depth would result in greater than 5 per cent error in the datum.

to zero; the same result is obtained via application of the Green's function to the sensitivity eq. (2). Similarly, with respect to receiver position, $\partial\phi(\mathbf{r}, \mathbf{r}_s)/\partial x = I\partial G(\mathbf{r}, \mathbf{r}_s)/\partial x$ such that the perturbation of potential due to mislocation of the receiver and source electrodes is given, to the first order, by the directional derivative $\Delta\phi = I\nabla_s G \cdot \Delta\mathbf{r}_s + I\nabla G \cdot \Delta\mathbf{r}$. Since an analytical solution to the Green's function is not possible for heterogeneous media, the partial derivatives must be calculated by a differencing of offset Green's functions. Furthermore, for the typical case in which the Green's function is obtained via forward solution of the reciprocal problem (e.g. LaBrecque *et al.* 1999), the Green's function solution for the potential perturbation will ultimately equate to finite-differencing of multiple forward solutions of the potential.

To calculate the potential, we implement a weak-form, finite-volume solution (Dey & Morrison 1979) with singularity removal

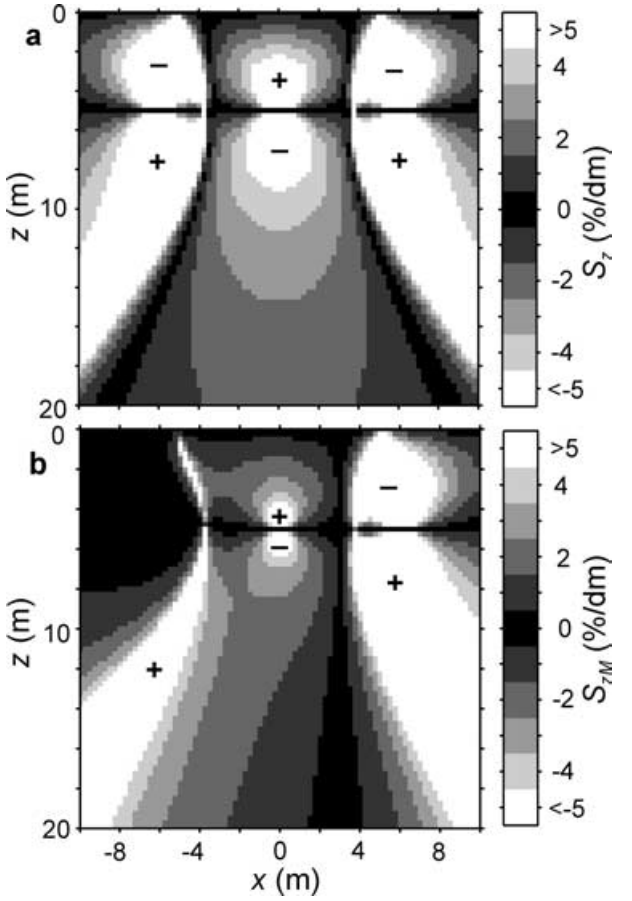

Figure 3. (a) Normalized sensitivity of potential difference to vertical position of the receiver dipole for a horizontal 6 m dipole–dipole experiment. The current dipole has electrodes at $x = \pm 3$ m, $z = 5$ m. Sensitivities are plotted at the receiver dipole centre. For example, a 10 cm vertical mislocation of a common-hole receiver dipole at 10 m depth would result in approximately 4 per cent error in the datum. (b) Normalized sensitivity of potential difference to vertical position of only the positive (left) electrode *M* of the receiver dipole.

of the point source function (Lowry *et al.* 1989). For a particular source, the sensitivity to the *k*th receiver position is approximated using the second-order accurate, centred finite-difference

$$\frac{\partial\phi}{\partial x_k} \approx \frac{\phi\left(\mathbf{r}_k + \Delta^p x\hat{\mathbf{i}}, \mathbf{r}_s\right) - \phi\left(\mathbf{r}_k - \Delta^n x\hat{\mathbf{i}}, \mathbf{r}_s\right)}{\Delta^p x + \Delta^n x}, \tag{7}$$

where $\Delta^p x$ and $\Delta^n x$ are the local positive and negative step sizes for a non-uniform numerical mesh.

Furthermore, the self-adjoint or reciprocal nature of the diffusion equation (Gangi 2000) results in the equality $\partial\phi/\partial x_s = [\partial\phi/\partial x]_R$ where R denotes the reciprocal experimental geometry obtained by swapping the source and receiver positions. For any experiment in which all electrodes are addressed as current electrodes at some point in time, the reciprocity relation implies that we need only calculate the sensitivity with respect to either the source or the receiver position. Since the forward solution is typically solved over all space at a grid spacing that is finer than the source spacing, it is most efficient to calculate sensitivities in terms of the receiver electrode positions only.

In the case of homogeneous media, the analytical Green's function is known and we can construct the position sensitivities from the

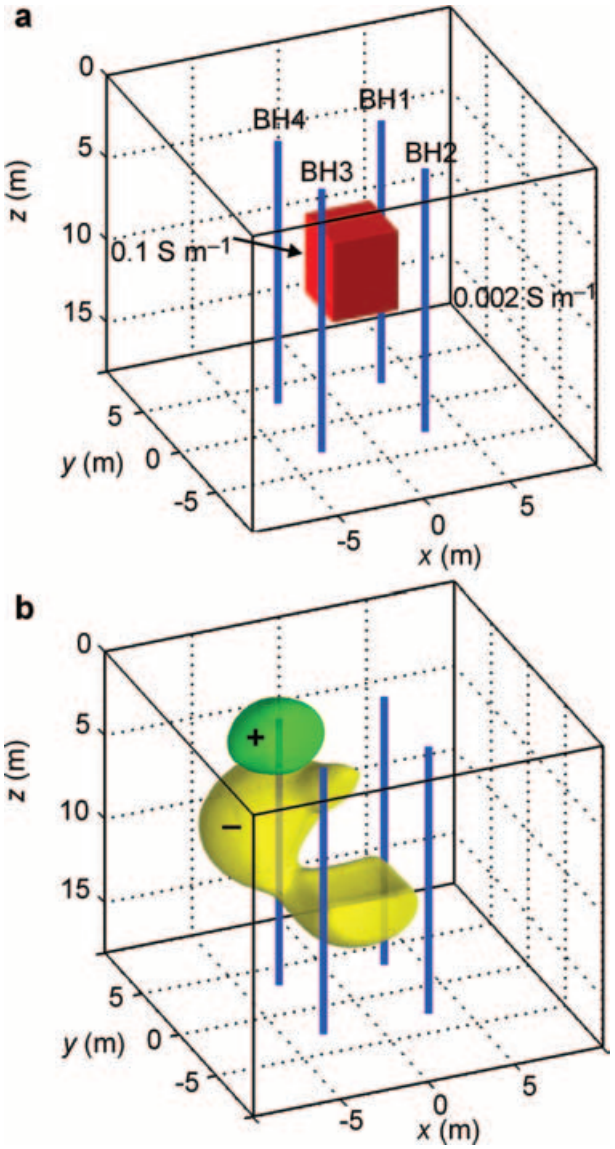

Figure 4. (a) Synthetic experimental geometry. (b) Sensitivity of potential to vertical receiver position for a pole–pole experiment. The figure illustrates perturbation of the ±1 per cent/dm sensitivity isosurfaces for a source electrode at 5 m depth in BH4.

exact expressions

$$\nabla_s\phi = \frac{I}{4\pi\sigma}\left(\frac{\mathbf{r}-\mathbf{r}_s}{|\mathbf{r}-\mathbf{r}_s|^3} + \frac{(x-x_s)\hat{\mathbf{i}} + (y-y_s)\hat{\mathbf{j}} - (z+z_s)\hat{\mathbf{k}}}{|\mathbf{r}-\mathbf{r}_i|^3}\right), \tag{8a}$$

$$\nabla\phi = -\frac{I}{4\pi\sigma}\left(\frac{\mathbf{r}-\mathbf{r}_s}{|\mathbf{r}-\mathbf{r}_s|^3} + \frac{\mathbf{r}-\mathbf{r}_i}{|\mathbf{r}-\mathbf{r}_i|^3}\right), \tag{8b}$$

where the image source is located at $\mathbf{r}_i = x_s\hat{\mathbf{i}} + y_s\hat{\mathbf{j}} - z_s\hat{\mathbf{k}}$.

ANALYTICAL RESULTS

The relative sensitivity of potential to receiver electrode position in the vertical direction (denoted as g_z) for a single source in a pole–pole experiment is illustrated in Fig. 1. Examples of receiver position sensitivities for vertical common-hole and horizontal cross-hole dipole–dipole experiments are illustrated in Figs 2 and 3, respectively.

To contextualize the sensitivity magnitudes, we note that measurements for ERT experimental setups are highly repeatable to less than 1 per cent (LaBrecque & Yang 2001). A better measure of random noise is given by reciprocal data and a common quality control procedure consists of a reciprocal data check and a culling of data that do not have reciprocal matches below some critical cut-off near 3–5 per cent (Zhou & Dahlin 2003). Due to the principle of reciprocity (Gangi 2000), data error associated with electrode mislocations are not caught and eliminated by reciprocal checks. Systematic errors associated with electrode mislocation are propagated via incorrect forward modelling and are, therefore, invisible to any noise-removal techniques that rely on identifying random noise.

If we assume 3 per cent to be the nominal critical error, then it is apparent from Fig. 1 that, for a 10 cm mislocation, the data for the pole–pole experiment will be significantly contaminated if they are acquired within approximately 3–5 m from the source in the vertical direction or 3 m from the source in the horizontal direction (not shown). It is also evident by comparing Figs 1, 2 and 3 that the sensitivity with respect to dipole receiver position (denoted as S_z) is greater than that for a pole receiver and also that the horizontal dipole data are less susceptible to position error than the vertical dipole data.

Since the homogeneous relative sensitivities are purely geometrical and independent of current strength or conductivity, the highly localized nature of the sensitivities for these simple examples illustrates that electrode position errors are particularly important for overlapping-scale problems. Significant sensitivities are limited to the very near-field, a region often occupied in near-surface environmental and engineering geophysical experiments.

SYNTHETIC RESULTS

For the case of heterogeneous media, we consider a simple synthetic ERT experiment consisting of four shallow boreholes enclosing a conductive target at depth (Fig. 4a). The experiment is designed as an approximation to a general near-surface contaminant detection and monitoring application. The boreholes are arranged in a square pattern 6 m on each side and extend to 20 m depth. The target has a conductivity of 0.1 S m^{-1}; the background conductivity is 0.002 S m^{-1}. Dimensions of the target are 4 m on each side in the horizontal directions and 5 m in the vertical direction between 6 and 11 m depth. Electrodes are placed at 1 m intervals in each borehole from 2 to 20 m depth and we will consider the synthetic data collected from a pole–pole experiment, a circulating vertical dipole–dipole experiment with 1 m dipoles, and a cross-borehole horizontal dipole–dipole experiment using the borehole pairs BH1–2, 2–3, 3–4 and 4–1.

The heterogeneous conductivity field acts to perturb the sensitivity of potential to the receiver position. As illustrated in Fig. 4(b), the conductive body acts to deflect the sensitivity isosurfaces. Conversely, a resistive body tends to channel or absorb the sensitivity distribution (not shown). To quantify the effects of electrode mislocations on the ERT data, we can examine the results for the synthetic experiments both spatially in terms of measurements down the boreholes and holistically in terms of frequency distributions.

The effects of receiver mislocation are illustrated in Fig. 5 for the synthetic data corresponding to a single source of a pole–pole experiment. Although the magnitudes of the errors associated with electrode mislocations are generally smaller than the perturbation

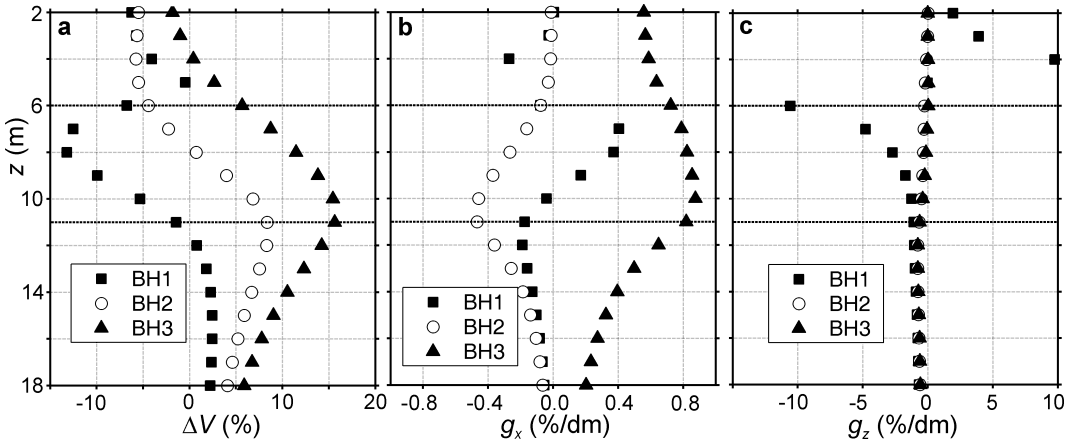

Figure 5. Pole–pole synthetic experiment with the source located at 5 m depth in BH1. (a) Relative change in data from homogeneous background condition. Relative sensitivity of data to (b) horizontal and (c) vertical receiver position. Dashed lines indicate vertical limits of heterogeneity.

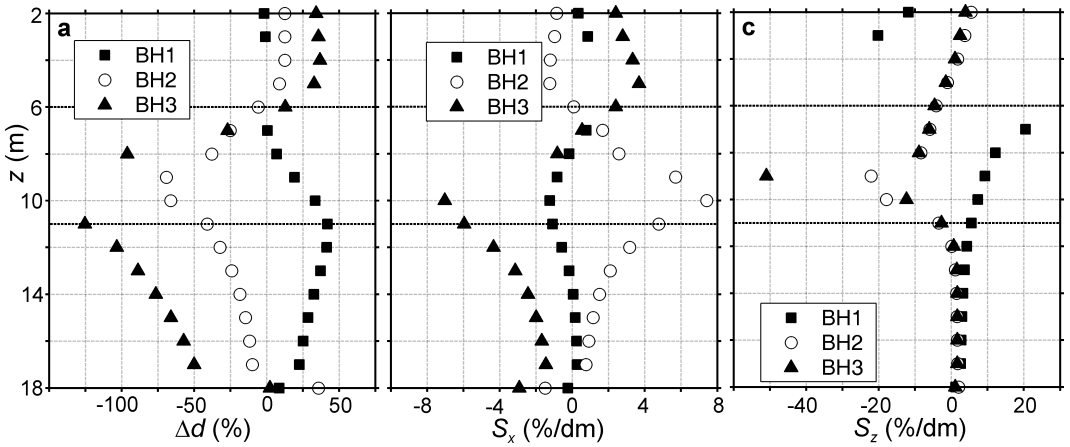

Figure 6. Vertical dipole–dipole synthetic experiment with the source dipole centred at 5.5 m depth in BH1. (a) Relative change in data from homogeneous background condition. Relative sensitivity of data to (b) horizontal and (c) vertical receiver dipole position. Quantities are plotted at the uphole electrode.

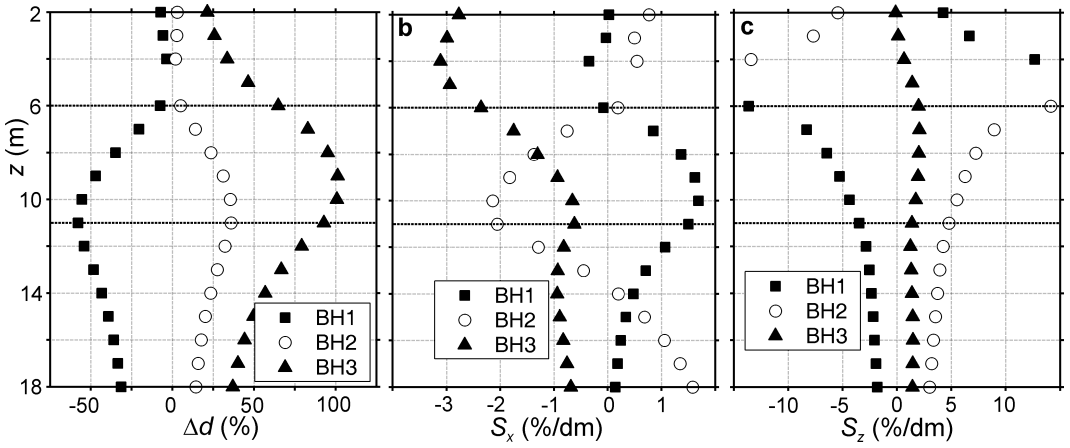

Figure 7. Horizontal cross-borehole synthetic experiment with the source dipole at 5 m depth spanning BH1 and BH2. (a) Relative change in data from homogeneous background condition. Relative sensitivity of data to (b) horizontal and (c) vertical receiver dipole position. Quantities are plotted at the positive receiver electrode.

of the data due to the heterogeneous body, errors within the source borehole are above experimental precision and comparable to typically estimated noise levels or reciprocal tolerances. In the non-source boreholes, errors are largest near the conductivity contrast but are of minimal magnitude. For the vertical dipole–dipole data (Fig. 6) and the horizontal cross-borehole data (Fig. 7), observed effects are more significant in that errors in the non-source boreholes are comparable to estimated noise levels and, in the near-field

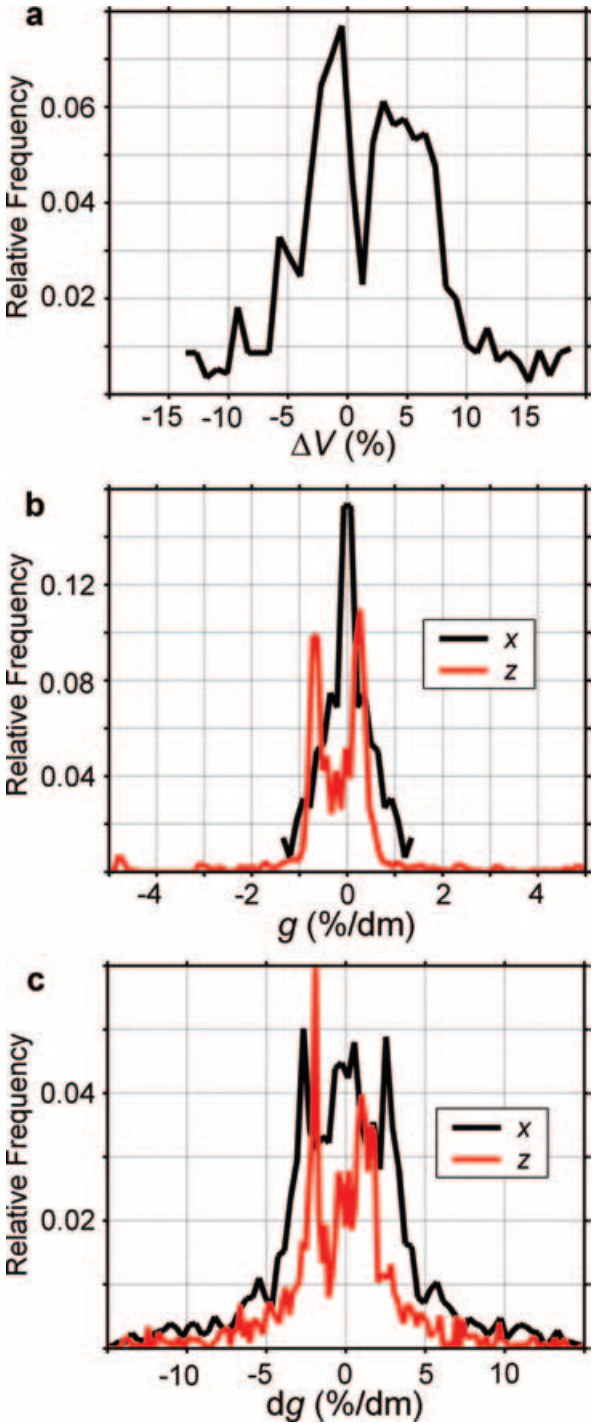

Figure 8. Distribution of (a) the relative change in the data from a homogeneous background, (b) the relative sensitivity of the data to receiver position, and (c) the relative sensitivity of the differenced data to receiver position for the pole–pole experiment. The legends *x* and *z* indicate sensitivity in the horizontal and vertical directions, respectively.

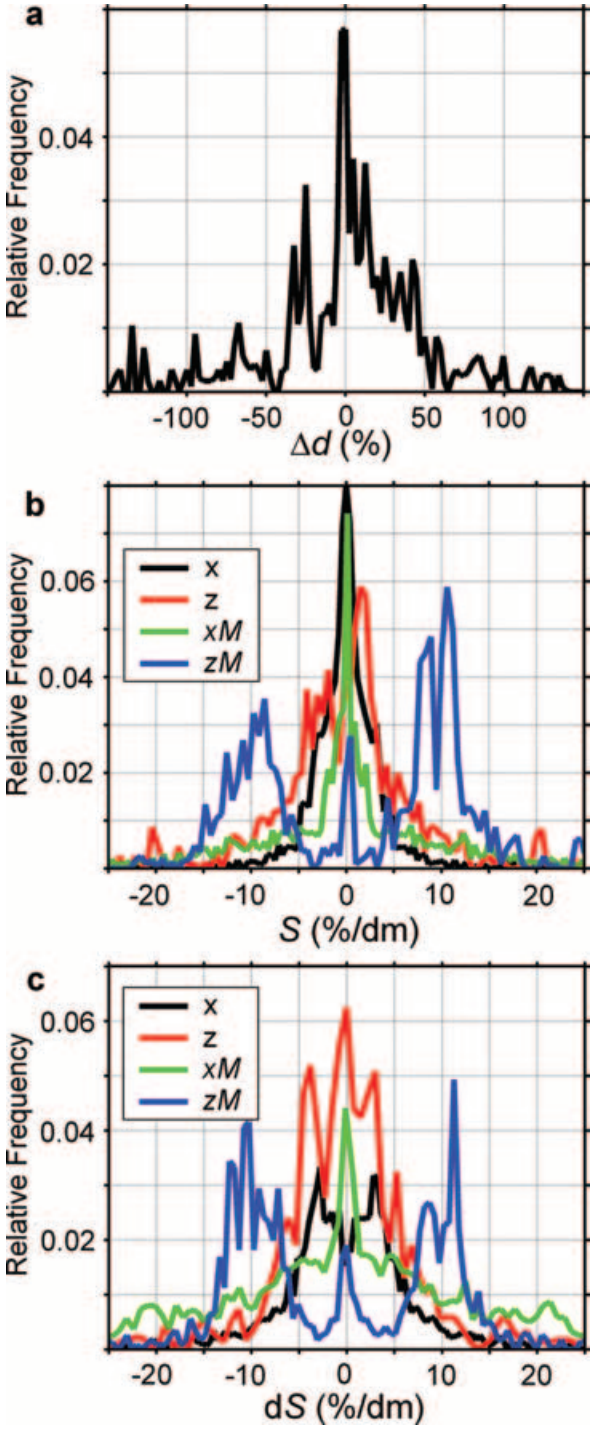

Figure 9. Distribution of (a) the relative change in the data from a homogeneous background, (b) the relative sensitivity of the data to position of the receiver dipole and the positive receiver electrode *M* and (c) the relative sensitivity of the differenced data to position of the receiver dipole and the positive receiver electrode for the vertical dipole–dipole experiment. The legends *x* and *z* indicate sensitivity in the horizontal and vertical directions, respectively.

region, the electrode mislocation errors are comparable to the signal strength associated with the heterogeneous body. As suggested by the analytical results, electrode mislocations are of greater concern for dipole data than for pole data. The largest errors are encountered for the vertical dipole–dipole experiment. For both the horizontal and vertical dipole–dipole experiments, the data are more sensitive to vertical as opposed to horizontal dipole position.

The complete data sets for each experiment are presented as relative frequency distributions in Figs 8–10. The frequency

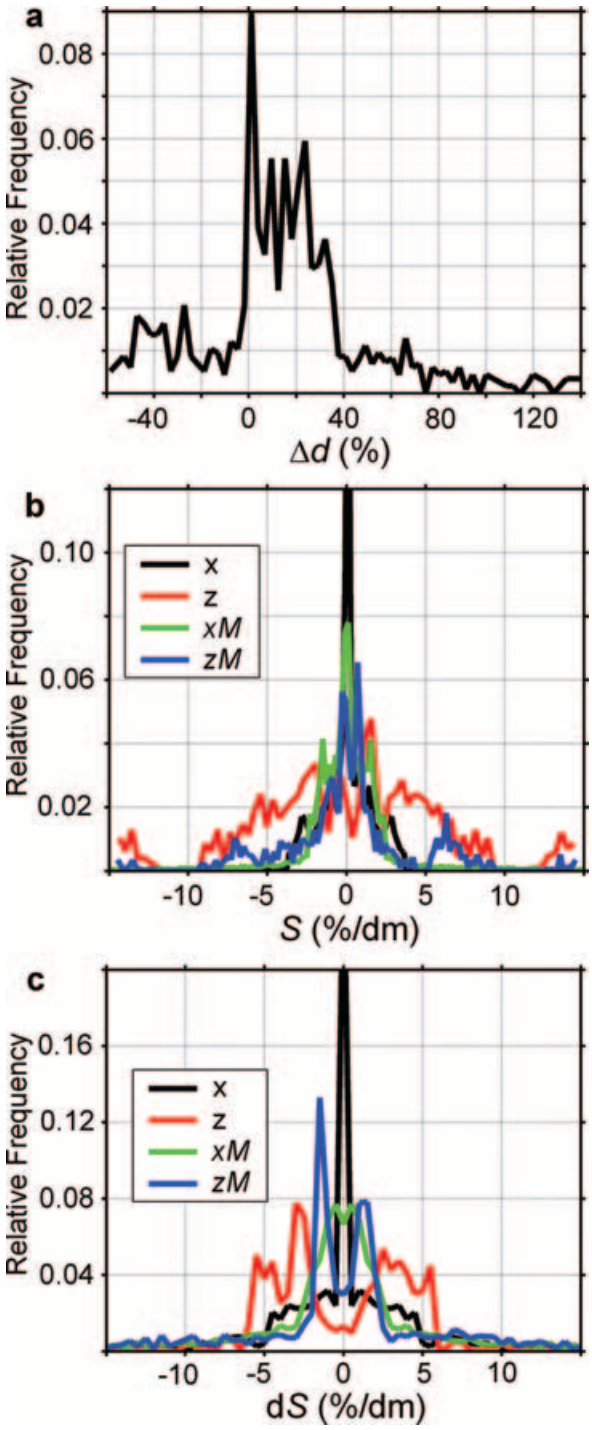

Figure 10. Distribution of (a) the relative change in the data from a homogeneous background, (b) the relative sensitivity of the data to position of the receiver dipole and the positive receiver electrode M, and (c) the relative sensitivity of the differenced data to position of the receiver dipole and the positive receiver electrode for the horizontal cross-borehole experiment. The legends x and z indicate sensitivity in the horizontal and vertical directions, respectively.

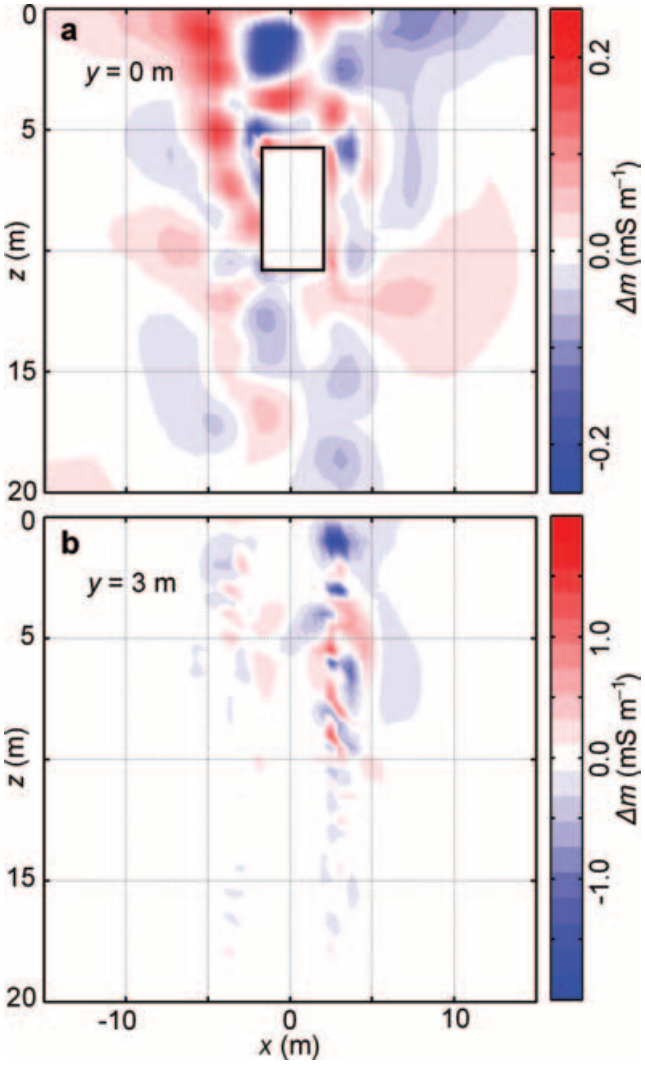

Figure 11. Pole–pole conductivity artefact distributions in the planes of (a) the target ($y = 0$ m) and (b) the mislocated electrode ($y = 3$ m) for a 0.25 m vertical mislocation of the uppermost electrode of BH1. Location of the conductive target is outlined.

distributions illustrate the overall statistical nature of the errors for a given survey geometry and data type. Overall, vertical dipole data appear to be the most susceptible to electrode mislocation. The vertical dipole data are most sensitive to vertical mislocation of only one electrode of the receiver dipole rather than to mislocation of the entire dipole. Conversely, the horizontal cross-borehole data are most sensitive to mislocation of the entire dipole. Perhaps most importantly, the frequency distributions reveal that the errors associated with electrode mislocations may not follow a normal distribution. In fact, we observe complicated, multimodal distributions, especially for the vertical (Fig. 9b) and horizontal (Fig. 10c) dipole experiments, that will introduce bias into the ERT data and the reconstructed electrical conductivity.

The frequency distributions also illustrate the effects of electrode mislocation on the differenced or time-lapsed experiment for which the data are considered to be the difference between pre- and post-event measurements (LaBrecque & Yang 2001). In this case, the background conductivity field is homogeneous and the perturbed conductivity field consists of the background plus the conductive target that could be representative of a contaminant plume that has migrated into the domain. The postulate of data differencing is that, if the pre- and post-event systematic errors (or position sensitivities) are very similar or the same, then the systematic error in the differenced data will be very small or zero. However, differencing

inevitably reduces the dynamic range of the data such that, in the event of incomplete cancellation, relative sensitivity may not be decreased. This is the case for the dipole-type geometries for which the relative position sensitivity distributions remain fairly constant for differenced data (Fig. 9b versus c and Fig. 10b versus c). However, for the pole–pole geometry, the pre- and post-event sensitivities are sufficiently different that data differencing leads to a significant increase in the potential for electrode mislocation error (Fig. 8b versus c). Systematic errors associated with electrode mislocations are not cancelled by data differencing.

CONDUCTIVITY ARTEFACTS

For a hypothetical mislocation of a particular electrode, we calculate the perturbation in potential for all measurements associated with that electrode and we predict the total systematic error of the data by superposition. Given the systematic error vector $\mathbf{e}^s$, we estimate the conductivity artefacts $\Delta\mathbf{m}$ according to $\Delta\mathbf{m} = \mathbf{J}^{-1}\Delta\mathbf{e}^s$, where $\mathbf{J}$ is the discrete Fréchet derivative matrix of the forward operator. We calculate $\mathbf{J}$ using an adjoint Green's function solution (e.g. Spitzer 1998) and solve for $\Delta\mathbf{m}$ via conjugate gradients with least squares (Golub & Van Loan 1996). It is important to note that not only is $\mathbf{J}$ model dependent, but it is also highly dependent on the number, location, and type of data. That is, $\mathbf{J}$ is both model and experiment dependent and, thus, it is difficult to make generalizations regarding artefact distributions. Artefacts estimated using the method presented here will differ from artefacts encountered in a full inverse procedure in so far as we do not consider Tikhonov-type model regularization and we utilize the exact conductivity for calculation of $\mathbf{J}$. Artefact distributions presented hereafter are local about the true model, whereas, in an inverse procedure, the position errors and associated artefacts may alter the convergence path of the non-linear solution.

The conductivity artefacts associated with a 0.25 m vertical mislocation of only the uppermost electrode in BH1 are illustrated in Fig. 11 for the synthetic pole–pole experiment. Artefacts are not limited to the vicinity of the mislocated electrode because the data associated with the mislocated electrode involve all of the electrodes in the other boreholes. Trends that persist for different models and experimental geometries are the concentrations of high magnitude artefacts in the vicinities of mislocated electrodes, boreholes and contrasts in conductivity. For example, in Fig. 11, we see that the upper right portions of the images tend to be more contaminated than the lower left regions and both the boreholes and target boundaries are evident as foci of artefacts.

For this example, artefact magnitudes are on the order of the background conductivity in the plane of the borehole and on the order of 10 per cent of the background conductivity in the plane of the target. Thus, position error artefacts will be more problematic when attempting to assess background variability than when merely identifying a conductive target. However, the artefacts do have the potential to inhibit accurate predictions of target boundaries and material properties. Furthermore, as the conductivity contrast decreases, the target will become more susceptible to contamination and a resistive target will exhibit a concentration of artefacts within the anomalous body. Finally, the example presented is for mislocation of a single electrode in a 3-D medium. Incorporation of additional electrode mislocations (such as borehole deviation) results in additive error and construction of $\mathbf{J}$ for a 3-D source in a 2-D earth (such as for 2-D ERT) results in an order of magnitude increase in synthetic conductivity artefacts.

CONCLUDING REMARKS

We have shown that for overlapping-scale experiments such as those typical of near surface environmental and engineering applications, electrode mislocations can significantly contribute to systematic data error. Awareness of this potential error is critical because electrode position errors will not be eliminated by reciprocal data filtering, but rather, will propagate through inaccurate forward modelling of the data.

For a synthetic experiment, we predict the systematic error due to electrode mislocation based on calculations of the sensitivity of the electrical potential to the source and receiver functions. Pole–pole data appear most robust to the effects of electrode mislocations except in a data differencing context. Horizontal dipole data appear less sensitive to electrode mislocations than vertical dipole data (possibly due to the increased dipole length). In most instances, the magnitude of the relative sensitivity to electrode position is well above typical noise levels but below the signal magnitude associated with the target. The errors exhibit complicated, multimodal statistical distributions that can depart significantly from a normal distribution. Data differencing does not reduce the susceptibility of the ERT experiment to electrode position errors when the potential field undergoes significant change between states. However, we have not considered site-specific signal-to-noise levels or the logistics of the different survey types or of data differencing that will undoubtedly play a factor in survey design.

Given predictions of the systematic data error, we utilize the local linearized Fréchet derivative of the inverse problem to estimate artefacts in the reconstructed electrical conductivity. We stress that specific results for heterogeneous media will be model dependent and, in the case of artefact distributions, experiment dependent. For the synthetic experiment considered here, we demonstrate that the contaminated data can result in inversion artefacts that populate large portions of the tomographic volume. Ultimately, in a similar fashion, the sensitivity of electrical potential to source and receiver position could be employed in a coupled inverse technique to recover small electrode mislocations.

ACKNOWLEDGMENTS

This research was funded by the Natural Sciences and Engineering Research Council of Canada (PGSB), the Inland Northwest Research Alliance (SSGP), EPA grant X970085-01-0, and NSF-EPSCOR grant EPS0132626. We thank the associate editor M. Everett and two anonymous reviewers for helpful comments and criticisms that greatly improved the manuscript.

REFERENCES

Aki, K. & Lee, W.H.K., 1976. Determination of three-dimensional velocity anomalies under a seismic array using first P arrival times from local earthquakes, 1, A homogeneous initial model, *J. geophys. Res.,* **81,** 4381–4399.

Binley, A., Cassiani, G., Middleton, R. & Winship, P., 2002. Vadose zone flow model parameterization using cross-borehole radar and resistivity imaging, *J. Hydrol.,* **267,** 147–159.

Daily, W. & Ramirez, L., 2000. Electrical imaging of engineered hydraulic barriers, *Geophysics,* **65,** 83–94.

Dey, A. & Morrison, H.F., 1979. Resistivity modeling for arbitrarily shaped three-dimensional structures, *Geophysics,* **44,** 753–780.

Ellis, R.G. & Oldenburg, D.W., 1994. The pole–pole 3-D DC-resistivity inverse problem, a conjugate gradient approach, *Geophys. J. Int.,* **119,** 187–194.

Gangi, A.F., 2000. Constitutive equations and reciprocity, *Geophys. J. Int.,* **143,** 311–318.

Golub, G.H. & Van Loan, C.F., 1996. *Matrix Computations,* 3rd edn, John Hopkins Univ. Press, Baltimore, MD.

Gough, D.O. & Sekii, T., 2002. On the effect of error correlation on linear inversions, *Mon. Not. R. Astron. Soc.,* **335,** 170–176.

Hohmann, G.W. & Raiche, A.P., 1988. Inversion of controlled-source electromagnetic data, in *Electromagnetic Methods in Applied Geophysics,* Vol. 1, pp. 469–503, ed. Nabighian, M.N., Soc. Expl. Geophys., Tulsa, OK.

LaBrecque, D.J. & Yang, X., 2001. Difference inversion of ERT data, A fast inversion method for 3-D in situ monitoring, *J. Env. Eng. Geophys.,* **6,** 83–89.

LaBrecque, D.J., Morelli, G., Daily, W., Ramirez, A. & Lundegard, A., 1999. Occam's inversion of 3-D electrical resistivity tomography, in *Three-Dimensional Electromagnetics,* pp. 575–590, eds Oristaglio, M. & Spies, B., Soc. Expl. Geophys., Tulsa, OK.

Li, Y. & Oldenburg, D.W., 1991. Aspects of charge accumulation in d.c. resistivity experiments, *Geophys. Prospect.,* **39,** 803–826.

Lowry, T., Allen, M.B. & Shive, P.N., 1989. Singularity removal, A refinement of resistivity modeling techniques, *Geophysics,* **54,** 766–774.

Maurer, H.R., 1996. Systematic errors in seismic crosshole data, Application of the coupled inverse technique, *Geophys. Res. Lett.,* **23,** 2681–2684.

McGillivray, P.R. & Oldenburg, D.W., 1990. Methods for calculating Fréchet derivatives and sensitivities for the non-linear inverse problem, A comparative study, *Geophys. Prospect.,* **38,** 499–524.

Morelli, G. & LaBrecque, D.J., 1996. Advances in ERT inverse modeling, *European J. Env. Eng. Geophys.,* **1,** 171–186.

Newmark, R.L., Daily, W.D., Kyle, K.R. & Ramirez, A.L., 1998. Monitoring DNAPL pumping using integrated geophysical techniques, *J. Env. Eng. Geophys.,* **3,** 7–13.

Ramirez, A., Daily, W., LaBrecque, D., Owen, E. & Chesnut, D., 1993. Monitoring an underground steam injection process using electrical resistance tomography, *Water Resour. Res.,* **29,** 73–87.

Shima, H., 1992. 2-D and 3-D resistivity image reconstruction using crosshole data, *Geophysics,* **57,** 1270–1281.

Slater, L.D., Brown, D. & Binley, A., 1996. Determination of hydraulically conductive pathways in fractured limestone using cross-borehole electrical resistivity tomography, *European J. Env. Eng. Geophys.,* **1,** 35–52.

Spitzer, K., 1998. The three-dimensional DC sensitivity for surface and subsurface sources, *Geophys. J. Int.,* **134,** 736–746.

Vasco, D.W., Peterson, J.E.Jr. & Lee, K.H., 1997. Ground-penetrating radar velocity tomography in heterogeneous and anisotropic media, *Geophysics,* **62,** 1758–1773.

Walker, S.E., 1999. Inversion of em data to recover 1-d conductivity and geometric survey parameter, *MSc thesis*, Univ. British Columbia, Vancouver, BC.

Yeh, J.T.-C., Liu, S., Glass, R.J., Baker, K., Brainard, J.R., Alumbaugh, D. & LaBrecque, D., 2002. A geostatistically based inverse model for electrical resistivity surveys and its applications to vadose zone hydrology, *Water Resour. Res.,* **38,** 1278, doi: 10.1029/2001WR001204.

Zhou, B. & Dahlin, T., 2003. Properties and effects of measurement errors on 2-D resistivity imaging surveying, *Near Surface Geophys.,* **1,** 105–117.